CHEMICAL ANALYSIS

A SERIES OF MONOGRAPHS ON ANALYTICAL CHEMISTRY
AND ITS APPLICATIONS

Editor
J. D. WINEFORDNER

VOLUME 155

WILEY-INTERSCIENCE

A JOHN WILEY & SONS, INC., PUBLICATION

New York • Chichester • Weinheim • Brisbane • Singapore • Toronto

Modern Analytical Methods in Art and Archaeology

ENRICO CILIBERTO AND GIUSEPPE SPOTO

Editors

Dipartimento di Scienze Chimiche
Università di Catania
Catania, Italy

WILEY-INTERSCIENCE

A JOHN WILEY & SONS, INC., PUBLICATION

New York • Chichester • Weinheim • Brisbane • Singapore • Toronto

This book is printed on acid-free paper.♾

Published simultaneously in Canada.

For ordering and customer service, call 1-800-CALL-WILEY.

Library of Congress Cataloging-in-Publication Data:
Modern analytical methods in art and archaeology / E. Ciliberto and G. Spoto, editors.
p. cm. — (Chemical analysis ; v. 155)
Includes index.
ISBN 0-471-29361-X (alk. paper)
1. Art—Expertising. 2. Chemistry, Analytic—Methodology. 3. Archaeological chemistry. I. Ciliberto, E. (Enrico) II. Spoto, G. (Giuseppe) III. Series.
N8558.M63 2000
702′.8′8—dc21 99-057435

Printed in the United States of America.
10 9 8 7 6 5 4 3 2 1

CHAPTER

6

PARTICLE-INDUCED X-RAY EMISSION

JEAN-CLAUDE DRAN, THOMAS CALLIGARO, and JOSEPH SALOMON

Laboratoire de Recherche des Musées de France, Paris, France

6.1. INTRODUCTION

Particle-induced X-ray emission (PIXE) is an ion beam analytical technique using a particle accelerator, generally an electrostatic one, single-ended or tandem with a voltage of a few megavolts, and allowing the determination of the concentration of the elements contained in a material by means of the emission of characteristic X-rays. X-ray production by a beam of charged particles was reported for the first time by Chadwick (1912), who bombarded various targets with alpha particles. The analytical use of this phenomenon had to wait more than half a century and the growth of semiconductor detectors to enable a true multielemental analysis by energy-dispersive X-ray spectrometry (EDS). This was initiated by Johansson et al. (1970), who gave its name to the technique. PIXE rapidly gained a great popularity because of its high sensitivity allowing trace element analysis down to about the 10-ppm level for most elements, thus some three orders of magnitude better than the electron microprobe. However, the quantification of the analyses was not straightforward, particularly for thick targets, due to complex matrix effects (ion energy loss, X-ray self-absorption, secondary fluorescence).

Sophisticated software programs are now able to take these effects into account so that an accuracy of about 10% can be routinely reached (Campbell et al. 1993).

PIXE applications to art and archaeology rapidly grew for two additional reasons:

1. PIXE is recognized as nondestructive and therefore meets the constraints linked to the uniqueness and precious character of museum

Modern Analytical Methods in Art and Archaeology, Edited by Enrico Ciliberto and Giuseppe Spoto. Chemical Analysis Series, Vol. 155
ISBN 0-471-29361-X

objects; this is due to the large cross section of the underlying phenomenon of inner shell ionization and thus to the low beam intensity and total ion dose necessary to the analysis.

2. The technique can be easily implemented in the external beam mode, that is, in air or preferably in a helium atmosphere, because it can stand some energy dispersion since the above-mentioned cross section varies smoothly with energy; external beam configuration allows the *in situ* analysis of large or fragile objects without the need of sampling or vacuum.

The scope of this chapter is to provide the basic knowledge for applications in the field of art and archaeology. For further information, the reader is referred to two extensive textbooks (Johansson and Campbell 1988; Johansson and al. 1995), book sections (Cohen and Clayton 1989), and numerous review articles (Mitchell and Barfoot 1981; Bird et al. 1983; Breese et al. 1992; Cahill 1980; Demortier 1991; Sciuti and Suber 1991; Swann 1997).

6.2. PHYSICAL PRINCIPLES

6.2.1. Production of Characteristic X-Rays

The PIXE technique relies on the emission of X-rays induced by the interaction of energetic light ions (most frequently protons of a few mega-electronvolts) with constituent atoms of materials. This interaction involves three successive steps:

1. An electron is expelled from an inner shell of the atom (inner shell ionization, e.g., the K shell, which is the deepest one containing two electrons).
2. The electronic vacancy is filled by an electron originating from a more external shell (e.g., the L shell, containing up to eight electrons distributed into three subshells L_1, L_2, and L_3).
3. The resulting excited state releases the excess electron binding energy $E_K - E_L$ by the emission of either an X-ray of this energy, characteristic of the target atom, or an Auger electron from a third electronic shell (e.g., M) with a kinetic energy $E_K - E_L - E_M$. The relative probability of X-ray emission is called the fluorescence yield ω and for the K lines varies from 0 to 1 when increasing the atomic number.

The emitted X-rays correspond to the electronic transitions (Fig. 6.1) predicted by quantum mechanics and follow the so-called selection rules based

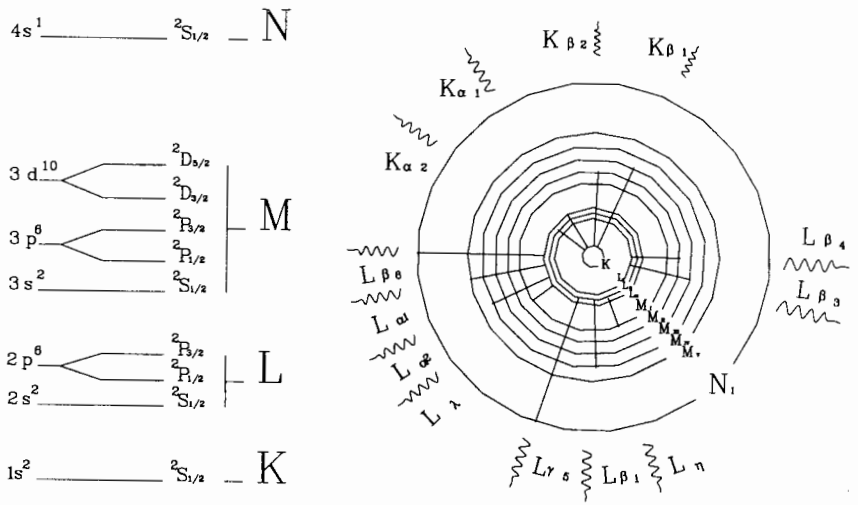

Figure 6.1. Scheme of electronic shell structure of Cu atom and associated transitions following primary ionization and leading to PIXE spectrum.

on the atom quantum numbers (n principal, l orbital angular momentum, j total angular momentum. These selection rules state that $\Delta n > 0$, $\Delta l = \pm 1$, $\Delta j = 0, \pm 1$. The multiplicity of the allowed transitions induces several discrete lines in the spectrum, grouped in series of decreasing energy: K lines, L lines, and so on, corresponding to the shells where occurred the primary ionization. Each series contains several components, for example, K_α and K_β (Siegbahn notation) of increasing order of energy but of decreasing intensity. The energy values of the components and the intensity ratios provide the fingerprint pattern that identifies the element. For a given series the X-ray energy steadily increases with the atomic number Z of the target atom, according to Moseley's law: $E = C(Z - s)^2$, where C is a constant different for each spectral series and s the shielding constant close to 1. Only K and L lines are used for analytical purposes. In EDS based on a silicon detector, the detector efficiency limits the range of useful X-rays from 1 to 40 keV. Therefore the useful energy range of the K lines extends from about 1 keV for sodium ($Z = 11$) to 37 keV for neodymium ($Z = 60$), and that of the L lines from 5 keV for neodymium to 13 keV for uranium ($Z = 92$).

6.2.2. Cross Section of X-Ray Production

For a given single-element target of atomic number Z, the cross section of the production of a given X-ray line is $\sigma^x = \sigma_z \omega_z b_z$, where σ_z is the cross section of primary inner shell ionization, ω_z the fluorescence yield, and b_z the

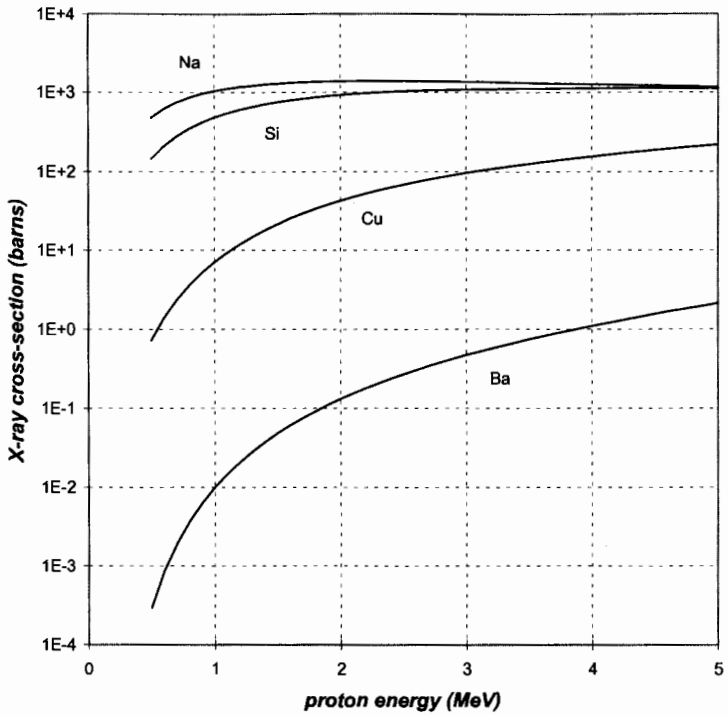

Figure 6.2. Variations of cross section of KX-ray emission with proton energy on several targets.

relative intensity of the line; ω_z and b_z are characteristic features of the atom and at least for the K lines do not depend on the ionization process, whereas σ_z is directly related to it. Particle-induced ionization follows roughly the same law as electron-induced ionization, namely the speed matching law, which states that σ^i is maximum when the velocity of the incident particle matches the orbital velocity of the electron in a given shell. Consequently for a given target, σ_z and σ^x increase with the energy E of the incident ion up to a maximum and then slowly decrease (Fig. 6.2). With protons and for most atoms except the lightest ones, the value of the maximum exceeds the practical energy range (2 to 3 MeV) set by background radiation (see the next section). At a given incident energy σ_z and σ^x for both the K and L lines rapidly fall when increasing the target atomic number Z (Fig. 6.3). For intermediate and heavy elements, L lines are clearly more favorable than K lines by several orders of magnitude. Ions heavier than protons must have the same speed as protons and thus the same energy per nucleon to have the same ionizing power; consequently, an energy of 48 MeV is needed for ^{16}O

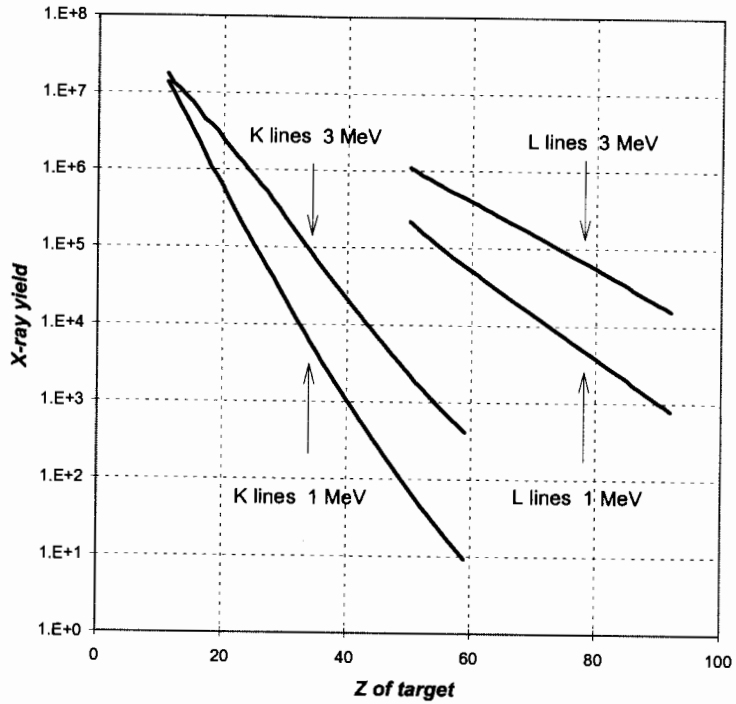

Figure 6.3. Variations of KX-ray yield with atomic number for thin targets of 1 μg/cm^2 thickness bombarded with 1 μc of 1- and 3-MeV proton beams.

ions, which is out of reach with small accelerators. However, heavy ions are sometimes used to induce multiple ionization, which can provide information on the chemical state of the target atom through satellite lines in the X-ray spectrum.

A universal scaling law for the cross section of K-shell primary ionization (Fig. 6.4) was successfully inferred from theoretical calculations, based on two models, the impulse or binary encounter approximation (BEA; Garcia et al. 1973) and the planar wave Born approximation (PWBA). The first model, based on classical mechanics, describes the ionization process as a direct collision between the projectile nucleus and the bound electron. The second model relies on the perturbation theory of quantum mechanics and considers the phenomenon as a transition from an initial state (plane-wave projectile and bound atomic electron) to a final one (plane-wave projectile and ejected electron). The PWBA model was notably improved and transformed into the ECPSSR model by Brandt and Lapicki (1981), who introduced several correction factors linked to the effects of the energy loss (E), the nuclear Coulomb field (C), the perturbation of the stationary atomic

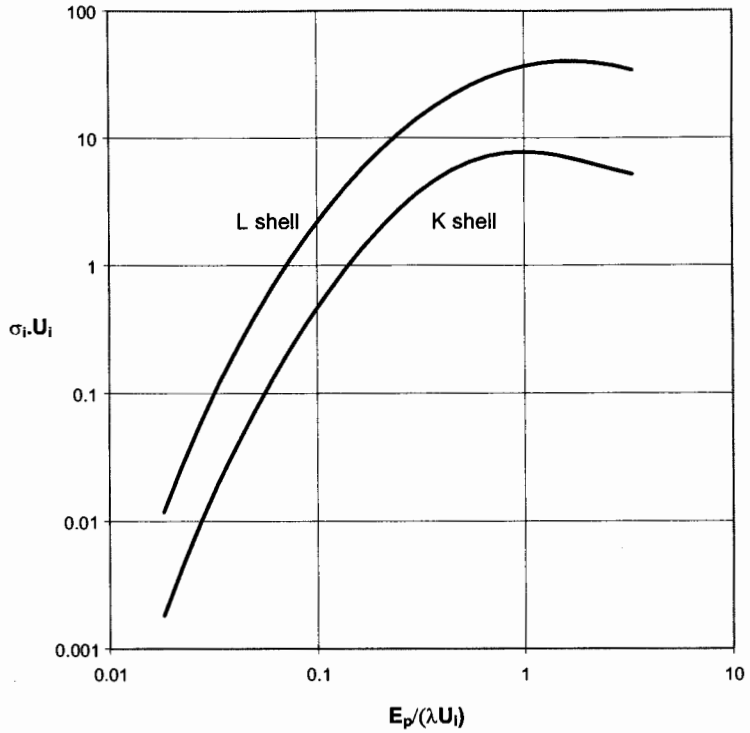

Figure 6.4. Universal scaling law for K- and L-shell ionization of elements calculated using polynomial fit of Johansson and Johansson (1976).

state (PSS) as well as relativistic effects (R). If one considers a projectile of nuclear charge Z_1, mass M, and energy E (in kilo-electron-volts), expelling a K-shell electron of binding energy U_K with a cross section σ_K, Figure 6.4 expresses the variations of $U_K{}^2\sigma_K/Z_1{}^2$ as a function of $E/\lambda U_K$ with $\lambda = M/m$ the ratio of the projectile mass to that of the electron. There is a good agreement between the theoretical calculations and a large amount of experimental data. One can also note a maximum for $E/\lambda U_K = 1$, which is another expression of the speed matching quoted above.

6.2.3. Background Radiation

As in other spectrometric techniques, the detection limit is set by the amplitude of the background. X-ray spectra induced by electrons exhibit, in addition to characteristic lines, a continuum due to the bremsstrahlung radiation originating from the slowing down of incident electrons during Coulomb

interactions with nuclei. This continuum extends to the energy of the incident electron, and its intensity is maximum at half this value. In the case of X-rays induced by protons, the bremsstrahlung directly produced by these particles is considerably reduced (the intensity being roughly inversely proportional to the square of the projectile mass). The only important source of bremsstrahlung is that due to secondary electrons. As the maximum energy transferred to electrons is $4Em/M$, where m and M are respectively the electron and projectile masses, the extension of this bremsstrahlung is directly related to the incident particle energy E. Thus, for a proton energy of 3 MeV, the background extends up to 6 keV. However, in the case of insulating targets, especially when analyzed under vacuum, charging effects can produce voltages of several tens of kilovolts with a subsequent acceleration of secondary electrons and extension of the background. As shown in the next section, the background radiation is not the sole limitation to the sensitivity of the technique; several other phenomena that can be called instrumental artifacts occur that can markedly blur the spectra. They are directly related to X-ray interaction with the semiconductor detector, most often a Si(Li) detector.

6.3. X-RAY DETECTION

6.3.1. Detector Characteristics

PIXE analysis generally relies on EDS using semiconductor detectors (most often a silicon crystal in which lithium has drifted) that convert the X-ray photons into electron–hole pairs, resulting in voltage pulses of height proportional to the photon energy. However, the efficiency of this process is not constant over the entire energy range, due mostly to the detector structure and dimensions. A schematic cross section of a Si(Li) detector is shown in Figure 6.5, taken from Potts (1987). The crystal is connected to a liquid nitrogen cryostat via a copper cold finger and is mounted in a special housing hold under high vacuum and terminated by a very thin window made of a low-Z material, usually a Be foil a few micrometers thick. The presence of such a window restricts the energy of detectable X-rays to a minimum of about 1 keV corresponding to the K X lines of Na. On the other side of the energy range, the detector thickness (from 2 to 5 mm) is not sufficient to stop all photons and thus its efficiency drops steeply (Fig. 6.6).

Another important parameter is detector resolution, which characterizes its ability to separate X-ray lines of very close energy values. It is usually expressed as the full width at half maximum (FWHM) of a reference photopeak, namely that corresponding to the Mn K_α line at 5.9 keV emitted by a

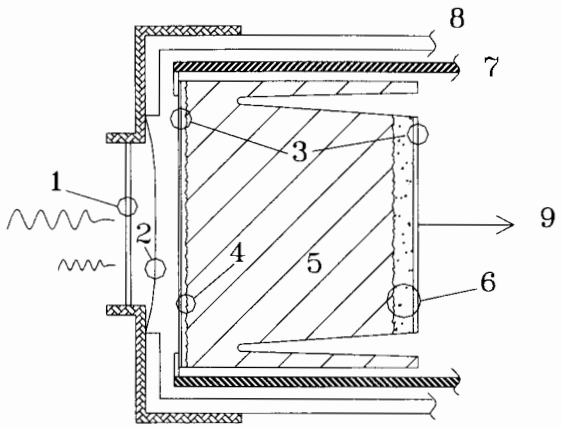

Figure 6.5. Schematic view of typical Si(Li) detector (Potts 1987): (1) filter (various materials and thicknesses); (2) thin window (generally about 10 μm Be); (3) Au front and rear contact layers (0.02 μm); (4) Si dead layer (0.03–0.1 μm); (5) detector crystal (3–5 mm); (6) Li diffusion layer (300 μm); (7) support connected to Cu cold finger; (8) detector housing; (9) signal to field effect transistor.

^{55}Fe radioactive source. Current Si(Li) detectors have a resolution in the range 140 to 160 eV.

6.3.2. Detection Artifacts

In a typical PIXE spectrum as that represented in Figure 6.7, one notes beside the K and L lines of copper, the following features purely instrumental (from the low- to the high-energy sides):

1. *Escape Peaks.* Small peaks distant from the corresponding K or L lines of an energy difference of 1.74 keV (exactly the energy of the Si K X-rays). These peaks derive from incomplete conversion of the X-photons into electron–hole pairs. Indeed, these photons undergo the photoelectric absorption within the detector, most often by interaction with an electron of the Si K shell. The expelled electron collides with other Si atoms producing further electron–hole pairs. The original Si atom deexcites by emitting either a Si K X-ray or an Auger electron, which are both likely to be absorbed within the detector active volume in such a way that the full energy of the primary photon is deposited in the detector. However, when the primary ionization occurs close to the detector surface, there is a significant probability that the Si K X-ray escapes without further ionization. The amplitude of such escape peaks is usually lower than 1% of the main peak.

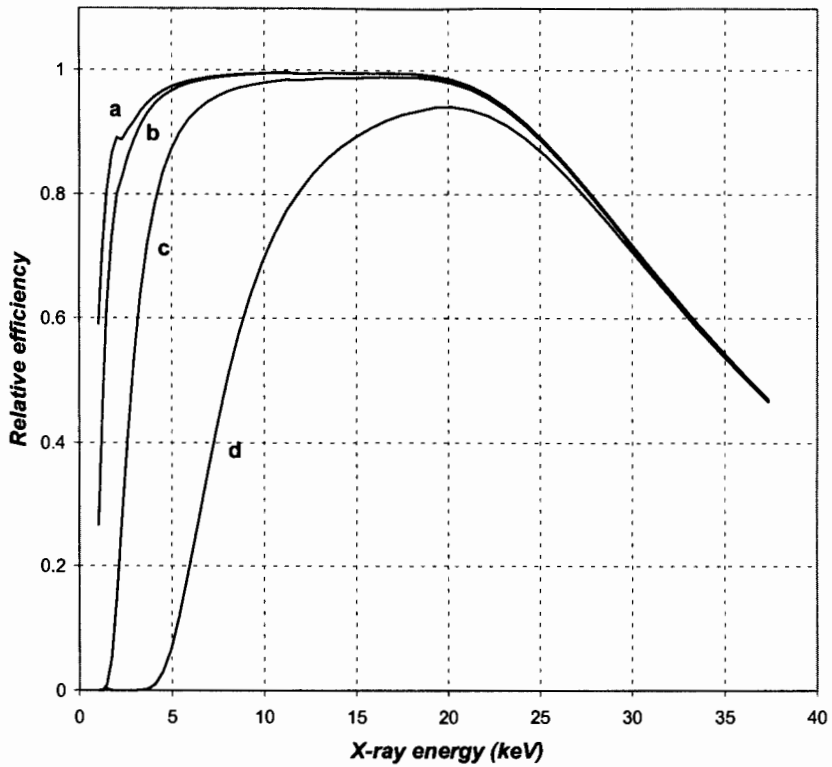

Figure 6.6. Variations of efficiency of a Si(Li) detector with X-ray energy: (*a*) Si(Li) crystal alone with 0.01-μm Au contact layer and 0.1-μm dead layer; (*b*) addition of 8-μm Be window; (*c*), (*d*) addition of either 125-μm Be or 50-μm Al filter.

2. *Pileup Peaks.* These peaks arise from the inability of the electronic system to separate coincident pulses of distinct energies E_1 and E_2. If the time interval between two incoming X-rays is shorter than the pulse shape of the amplifier, the two corresponding pulses are summed together, yielding a continuum from E_1 to E_2 up to $E_1 + E_2$. If the pulse processor is able to reject pairs of pulses in such a situation, it will still remain a small peak at energy $E_1 + E_2$, corresponding to the simultaneous detection of the two X-rays. The count rate of the pileup peak is $C_p = 2\tau C_1 C_2$, where C_1 and C_2 are the count rates of the two X-rays and τ the resolving time of the amplifier.

3. *Compton Continuum.* Such a continuum mostly originates from the Compton effect undergone on the sample and the Si detector by the gamma rays induced by proton interaction with light nuclei, mostly Na, Al, and Si and to a lesser extent F. This last feature also explains the limitation to 3

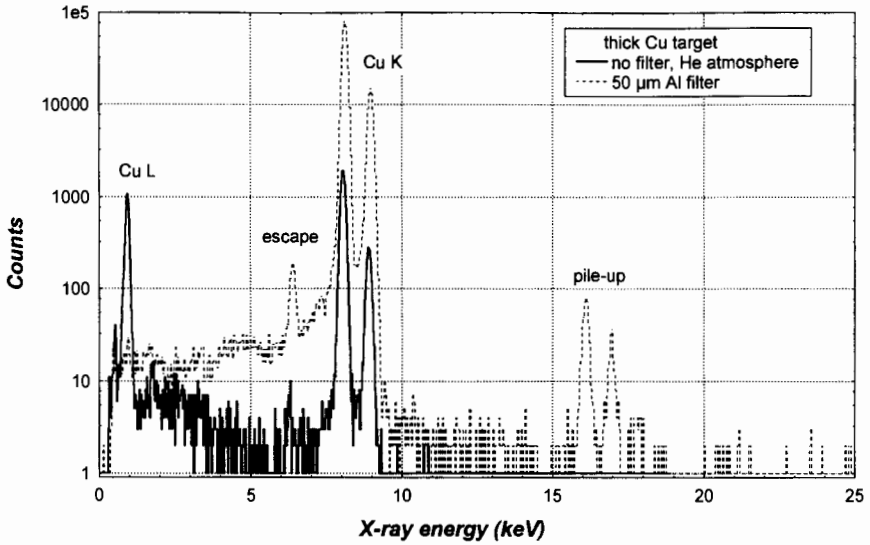

Figure 6.7. PIXE spectrum of copper thick sample obtained with Si(Li) detector and showing various detection artifacts.

MeV of the incident proton energy: above this value the probability of nuclear reactions with gamma ray emission is notably increased.

4. *Peak Tailing.* The response of a Si(Li) detector to a monochromatic X-ray source is modeled by a Gaussian peak, and on the low-energy side by one or two exponential tails and a flat plateau (see Section 6.7). The low-energy tail affects the detection limit of elements with X-ray lines of lower energy than the matrix ones. For example, this is the case of metallic alloys containing high concentration of heavy elements such as Hg, Au, and Pb. Moreover, the peak tailing features are characteristic of each detector and must be accurately measured at regular time intervals because of possible evolution, in order to perform a real quantitative analysis.

6.4. YIELD–CONCENTRATION RELATIONSHIP

Quantitative analysis requires us to establish a reliable correlation between the number of counts Y_z in a particular X-ray line under given experimental conditions and the number of atoms per cubic centimeter, N_z, of the corresponding element of atomic number Z assumed to be uniformly distributed. The simplest situation occurs for a thin target for which both the energy loss of the incident protons (and the subsequent variation of the ionization cross

section) and the absorption of the X-rays of interest are negligible. This corresponds to a thickness of the order of 1 µm in light matrices leading to an attenuation of the Na K_α X-rays lower than 10%.

6.4.1. Thin Targets

The relationship between Y_z and N_z is quite straightforward:

$$Y_z = \frac{N_z t \sigma_z \omega_z b_z Q \varepsilon_z \Omega}{4\pi \cos\theta_i}$$

where t is the thickness of the target, Q the number of incident protons, ε_z the detector efficiency for the corresponding X-ray, Ω the detector solid angle, and θ_i the angle between the beam and the sample normal. Considering that

$$N_z = \frac{\rho C_z N_a}{A_z}$$

where ρ is the sample specific gravity, C_z the weight concentration of element Z, N_a the Avogadro number, and A_z the mass number, it comes

$$Y_z = \frac{\rho C_z t N_a \sigma_z \omega_z b_z Q \varepsilon_z \Omega}{4\pi \cos\theta_i A_z}$$

Putting $k_z = N_a \sigma_z \omega_z b_z \varepsilon_z \Omega / (4\pi \cos\theta_i A_z)$, which is a parameter independent of both the element content and the number of incident protons, defined as the thin target sensitivity for element of atomic number Z, the previous equation becomes

$$Y_z = k_z Q \rho C_z t = k_z Q M_z$$

M_z being the mass per unit area (in microgram per square centimeter). Therefore, knowing k_z and Q (generally expressed as the integrated proton charge in microcoulomb), the mass per unit area M_z can be deduced from the measured yield Y_z. Such an analysis is absolute and does not need the use of a standard. The accuracy can be better than 10% when using K lines due to the accurate knowledge of K-shell ionization cross sections but poorer with L lines. This method can be used to get an X-ray yield calibration curve, Y versus Z, characteristic of the analytical system. This is performed by means of a series of thin samples, monoelemental or compounds, vacuum deposited on a polymer foil. When an unknown element is detected and its X-ray yield measured, the use of the yield curve allows the determination of

the mass per unit area of the corresponding element. Once such a calibration curve has been established, it is valid as long as the analytical system is not modified.

6.4.2. Thick Targets

Two phenomena intervene to complicate the yield–concentration relationship. First, the incident protons progressively slow down within the sample from their initial energy E_0 to zero at the end of their range. Consequently, the cross section regularly decreases as a function of the depth x. The depth–energy relationship

$$x = \frac{1}{\rho}\int_{E_0}^{0} \frac{dE}{S(E)} \tag{6.1}$$

is inferred from the energy loss variations $dE/dx = -\rho S(E)$ in which $S(E)$ is the matrix stopping power. In addition, the X-rays produced at that depth are attenuated by the overlayer of material. The calculation is performed by dividing the sample into successive thin layers and adding their contribution to the global X-ray production. The overall yield is expressed as

$$Y_z = \frac{\Omega Q \varepsilon_z \omega_z b_z N_a}{4\pi A_z}\int_{E_0}^{0} \frac{\sigma_z(E) T_z(E)}{S(E)}\, dE \tag{6.2}$$

where the integral corresponds to a correction factor that takes into account the depth variation of the cross section and the X-ray self-absorption, the transmission factor at a depth $x(E)$ being

$$T_z(E) = \exp\left[-\left(\frac{\mu}{\rho}\right)_z \frac{\cos\theta_i}{\cos\theta_o}\int_{E_0}^{E} \frac{dE}{S(E)}\right]$$

where θ_o is the detection angle with respect to the normal to the sample surface.

6.5. OPTIMIZATION PROCEDURES

The Si(Li) detectors and their associated electronics on which are based most PIXE facilities in operation suffer from intrinsic limitations:

1. a limited energy resolution;
2. relatively long duration of the pulses, which limits the count rate to about two thousand counts per second at most in order to avoid important pile-up;
3. intense peaks due to major elements that exhibit a tail on the decreasing energy side, which interferes with small peaks of trace elements of lower atomic numbers; and
4. a sensitivity to backscattered charged particles that tends to lower the resolution.

The above features can markedly reduce the detection limit, particularly in the case of relatively high atomic number matrices like metallic alloys. Different attempts have been made to overcome such difficulties, which are based on two principles:

1. Attenuate matrix X-rays by an adequate filter.
2. Reduce or even avoid the emission of matrix X-rays.

6.5.1. Filters

The presence of a filter in front of the Si(Li) detector is already needed as a protection against backscattered particles. As mentioned above, its role is also to attenuate the matrix X-rays in order to reduce both the count rate detrimental to the detector resolution and the background on the low-energy side of the corresponding peaks. However, the simultaneous attenuation of the lower energy X-rays emitted by light elements like Na, for example, cannot be avoided, but this can be minimized by choosing a selective filter, that is, containing an element with an X-ray absorption edge just below the X-ray energy of interest, generally one or two units of atomic number below that of the emitting matrix element. In some cases, the attenuation by the filter is excessive and does not allow the accurate measurement of the matrix element content together with those of minor and trace elements. To cope with this situation, a small hole is made on the filter in order to allow the partial detection of nonattenuated matrix X-rays. This type of filter configuration is called a pinhole, or funny, filter (Harrison and Eldred 1973). It should also be stressed that the use of a filter can induce unwanted interfering radiation: the X-ray lines of the filter constituent element. A secondary filter can then be superimposed to the first one in order to suppress them, leading to a multilayer structure for the filter (Swann and Fleming 1990).

6.5.2. Selection of Beam Energy

Early PIXE operations most often used two different proton energies and different filter thicknesses to optimize the analytical conditions. The following procedure was applied:

1. The matrix elements of usually low Z are first analyzed with 1-MeV protons using a filter of appropriate thickness to stop the backscattered particles (about 15 μm Be including the intrinsic detector window).
2. High-energy (3-MeV) protons are used for the analysis of high-Z elements, frequently at trace level concentration, with a sufficient detection limit. A thicker filter (about 50 μm Al) is then necessary, which also totally absorbs the X-rays emitted by matrix elements.

Considerable progress has been made these last years in order to enhance the analytical performance and reduce the number of steps necessary for a complete measurement. This is linked with the development of external beams (see Section 6.8.1) and the use of two X-ray detectors to cover the whole range of X-ray energy. Details will be given in Section 6.8.3 devoted to a short description of the external beam line of the accelerator facility of the Research Laboratory of the Museums of France in Paris (Fig. 6.8).

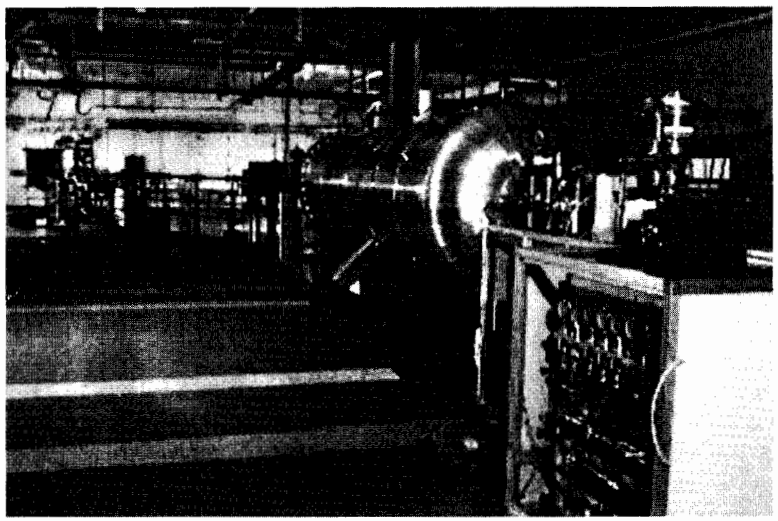

Figure 6.8. View of AGLAE IBA facility of Research Laboratory of the Museums of France.

6.5.3. Peculiar Setups

For some particular samples such as metallic alloys, current EDS setups are sometimes unable to separate interfering X-ray lines, whatever the number of beam energy values and the number of detectors. One solution would be to turn to wavelength-dispersive X-ray spectrometry (WDS), based on a Bragg crystal that provides a much better resolution than the Si(Li) detector for low-energy (1 to 5-keV) X-rays (Maeda et al. 1998), on the order of 10 eV for conventional crystals and even lower for special crystals. However, the technique would then lose its multielemental character, since each element must be measured separately. In addition, the count rate is considerably reduced, and consequently the duration of the measurements is markedly increased with subsequent greater risk of damage. Another way to avoid interferences it to selectively excite the X-ray line of the trace element of interest while avoiding the emission of matrix X-rays of higher energy. This favorable situation can be reached by irradiating a primary target of atomic number intermediate between those of the trace element and the matrix element and using the emitted X-rays to induce the trace element X-ray by fluorescence (Peisach 1987; Zeng et al. 1993); for example, a primary target of Ge produces K_α X-rays of 9.88 eV, sufficient to excite the K_α X-rays of Cu and Zn present at trace level in a lead matrix but not the interfering L_α lines of Pb (10.55 and 10.45 keV).

6.6. SPECTRUM PROCESSING BY COMPUTER CODES AND QUANTITATIVE ANALYSIS

6.6.1. Computer Codes

The use of sophisticated computer codes, such as GUPIX, GEOPIXE, PIXAN, and WitsHEX, is the key toward quantitative analysis by PIXE. These codes are the result of many years of effort and are being continuously improved, by incorporating the most recent theoretical developments (cross sections), accurate measurements of basic parameters (stopping powers for protons, X-ray attenuation coefficients, fluorescence yields), as well as the various instrumental artifacts (pile-up peaks, escape peaks, peak lineshape). We will briefly describe below the characteristics of the GUPIX program (Maxwell et al. 1988), which is now the most widely used.

6.6.2. Spectrum Synthesis

The response of the Si(Li) detector to a monochromatic X-ray is modeled by the sum of a Gaussian and at the low-energy side of an exponential tail and a

plateau (Campbell et al. 1987). Thus a monochromatic line ideally centered at channel c will give birth to a more complex structure where the content of any channel i can be numerically calculated. Five parameters, $a_1, \ldots, a_5$, defined hereafter, are characteristic of the detector. The first three are defined by the channel–energy relationship:

$$i(E) = a_1 + a_2E + a_3E^2$$

and the two others by the expression of the detector resolution:

$$\kappa(E) = \sqrt{a_4 + a_5E}$$

The escape peaks are calculated channel by channel using the following empirical formula (Johansson 1982):

$$\text{esc}(E - 1.742\ \text{keV}) = y(E)C_1\left[1 - T\log\left(1 + \frac{1}{T}\right)\right] \qquad T = C_2E^{C_3}$$

with $C_1 = 0.01896$, $C_2 = 0.009255$, $C_3 = 2.9662$, $1.84\ \text{keV} < E < 17.5\ \text{keV}$. The parameters $a_1, \ldots, a_5$ will be adjusted during the fitting procedure.

The overall theoretical spectrum of the sample is obtained by summing the contributions of all X-ray lines for each element and then for all elements detectable in the sample. Consequently, the content of each channel i of the spectrum is expressed by

$$y_i^{\text{sim}} = \sum_{z=\text{elements}} a_z \left[\sum_{c=K \text{ or } L \text{ lines}} R_{zc}\, y(i, c)\right]$$

The energies of the c lines are calculated from the binding energies of the electronic shells; R_{zc} is the relative height of the c line with respect to the main line (i.e., K_α or L_α) for element Z and a_z is a parameter proportional to the element concentration. Other spectrum features such as continuum background and pile-up peaks are also simulated with special numerical procedures.

6.6.3. Fitting Procedure

The processing of PIXE spectra is ruled by the same principle whatever the software package used. Assuming a given elemental composition, the program simulates a theoretical spectrum that is compared to the experimental one. The simulation parameters, in particular the sample composition, are optimized by iteration in order to reduce the gap between the two spectra.

6.6.4. Calculation of the Elemental Concentrations

To convert the peak heights a_z obtained above into concentrations C_z, it is necessary to know the yields Y_z under the experimental conditions and for a given matrix (proton energy, target composition, etc.). The theoretical relationship giving the yield Y_z per unit of weight concentration of element Z in a thick target is given by Eq. (6.1) and (6.2) of Section 6.4.

The data necessary for the calculation of this yield are the following:

Tabulated Data

ionization cross sections σ_z of K and L shells;
fluorescence yields ω_z of K and L lines;
X-ray attenuation coefficients μ_z; and
stopping powers $S(E)$.

Experimental Data

overall detector efficiency ε_z, including filters;
detector solid angle Ω; and
integrated charge Q.

The parameters ε_z and Ω are obtained by means of thin or thick standards or calibrated radioactive sources, while Q must be measured with a current integrator.

The concentration of element Z in the sample C_z^{spl} can then be deduced from the measured area of the main peak a_z:

$$C_z^{spl} = \frac{a_z}{Y_z}$$

This procedure is absolute if all the Y_z can be calculated, which requires us to know ε_z, Ω, and Q. In practice, these instrumental parameters are rather difficult to accurately assess. Consequently, one relies on procedures that bypass these parameters and reduce the sources of errors. These procedures are presented next.

Internal Standard. If one element of atomic number Z' present in the spectrum has a known concentration, the concentrations of all other elements can be deduced from the relation

$$C_z^{spl} = C_{z'}^{spl} \frac{a_z^{spl}}{a_{z'}^{spl}} \frac{Y_{z'}}{Y_z}$$

In the ratio of the yields Y the instrumental parameters Q and Ω vanish, and the matrix effects are those of the same matrix for different elements. However, it remains the ratio of the values of the detector efficiency for different elements. This procedure can be applied to samples that have been previously analyzed with a complementary technique [X-ray fluorescence spectrometry (XRF), scanning electron microscope (SEM), inductively coupled plasma (ICP)], which is seldom the case.

External Standard. This approach consists in using an external standard [National Institute for Standards and Technology (NIST), U.S. Geological Survey (USGS), or a sample previously analyzed] and comparing its PIXE spectrum to that of the sample. The concentration of element Z in the unknown sample is related to that in the standard by the formula

$$C_z^{spl} = C_z^{std} \frac{a_z^{spl}}{a_z^{std}} \frac{Y_z^{std}}{Y_z^{spl}}$$

This time, all the instrumental parameters vanish from the yield ratio. The main drawback of this method is the need to accurately know the proton dose Q received by both the standard and the sample. In order to apply this method to art and archaeology, it has been necessary to develop a reliable technique of beam monitoring in external beam mode.

Summing Up the Components to 100%. The concentrations of all components satisfy to the relation

$$C_z^{spl} = \frac{a_z / Y_z}{\sum_z a_z / Y_z}$$

which implies $\sum_z C_z^{spl} = 100\%$. Such a constraint substitutes to the measurements of Q and Ω, which is quite advantageous with an external beam for which Q is difficult to measure. The key point in this approach is the assessment of the detector efficiency. The method is checked a posteriori by applying it to standards. It is only applicable to samples for which all constituent elements appear in the spectrum. It is for example the case of metallic objects made of bronze, brass, or gold. It can be extended to samples based on oxides (e.g., stones, ceramics) by assuming that the sum of oxides is 100%.

6.7. CAPABILITY OF THE TECHNIQUE

The popularity of PIXE in various research fields stems from its analytical performances combined with the ease of operation and its nondestructive character. The main constraint is obviously the need of sophisticated and costly equipment and a well-trained technical staff. Let us recall the most important qualities of PIXE:

1. *Multielemental Character.* Almost all elements of the periodic table can be analyzed simultaneously with the exception of the lightest ones (H to Ne). However, PIXE is frequently combined with another ion beam analytical technique, called PIGE (particle-induced gamma ray emission) for the measurement of some light elements (F, Na, Al, Si).

2. *Sensitivity.* As stated earlier, PIXE is a very sensitive technique suitable for trace element analysis. The sensitivity depends on the experimental conditions and the sample chemical composition in major elements. In the best case, for thick targets, the detection limit of elements in the range $20 < Z < 30$ is of the order of 1 ppm. This limit is governed by the signal-to-background ratio of Si(Li) detectors. The mean detection limit (MDL) for each element is defined by

$$\text{MDL} = 3.29\sqrt{B}$$

where B is the value of the background taken within a region extending at three standard deviations at each side of the Gaussian. This MDL expressed in count number is converted into concentration by means of the yield Y.

3. *Accuracy.* Sources of errors are linked to each step of the spectrum processing. During the spectrum acquisition, the content of each channel has a statistical uncertainty and the dose measurement has a few percent uncertainty. The spectrum fitting is also the source of errors, but it is during the complex numerical calculations of the yields that the risk of errors is important. Whereas the theoretical and tabulated data are known with an accuracy better than 5% and the error linked to the numerical integration is negligible, the assessment of the overall detector efficiency is an important source of uncertainty. The filter transmission is hardly known with good accuracy, and at low energy the intrinsic efficiency of the detector is hardly measurable. This makes the analysis of light elements ($11 < Z < 15$) particularly difficult. Consequently, the concentrations measured on a thick sample have an accuracy of the order of 5 to 10%. This accuracy is generally sufficient for the study of objects of art and archaeology, which usually do not have a homogeneity better than 5 to 10%.

4. *Nondestructive Character.* This property is of particular significance when dealing with precious objects of cultural heritage. Under proper conditions of exposure to the proton beam (intensity below a few tens nanoamperes per square centimeter for a fixed millimeter-sized beam), and particularly in an external beam mode, most materials of interest stand

irradiation without any visible damage. Concern still remains for organic materials like paper, parchment, leather, or painting (Cahill et al. 1984; Zeng et al. 1990; Cheng et al. 1998), particularly with microbeams (Cookson 1988; McColm and Cahill 1991; Cholewa et al. 1991), but reducing the intensity and cooling the sample with a helium flow generally avoid any risk. Another beam effect should also be mentioned, namely the possible mobilization of sodium and other alkalis in silicate crystals and glasses with the risk of erroneous measurements (Campbell et al. 1997).

5. *Rapidity and Ease of Measurement.* It usually takes between 3 and 15 min to collect a PIXE spectrum. The processing time is of the same order. However, it should be stressed than the interpretation of data for archaeological purpose can be much longer.

On the other hand, the following limitations are worth mentioning:

1. *Lack of Information on the Chemical State.* PIXE is strictly elemental and for instance will provide the amount of Fe without the distinction between Fe^{2+} and Fe^{3+}.
2. *Analysis of Near-Surface Layer.* The maximum probed depth is a few tens of micrometers variable with the elements of interest and depending on the matrix composition. This fact can constitute a serious problem whenever one wishes to determine nondestructively the bulk composition of an altered archaeological object.

6.8. EXPERIMENTAL SETUPS

6.8.1. External Beam

A unique advantage of the PIXE technique is its easy implementation under nonvacuum conditions, that is, in air or even better in a helium atmosphere. The main reason is that contrary to others ion beam analytical techniques [Rutherford backscattering (RBS) or nuclear reaction analysis (NRA)], it does not require high-energy definition and can stand a significant energy straggling linked to the beam interaction with both the exit window and the atmosphere without losing its analytical performances. This is due to the smooth variation of the X-ray production cross section with energy. Therefore, very shortly after its invention, PIXE was applied in the external beam mode, originally for the analysis of biological samples but very soon also for that of archaeological objects (Seaman and Shane 1975; Katsanos et al. 1976; Deconninck and Bodart 1978; Williams 1984; Mando 1994). Beam extraction into air is achieved through an exit window designed to withstand

the atmospheric pressure. Such a window is made of a thin foil of various materials selected on the following grounds (Raisanen 1984; Anttila et al. 1985; Rauhala and Raisanen 1985):

1. Beside its good mechanical properties, it should not be sensitive to radiation damage.
2. The background radiation due to beam interaction with the window should be minimized.
3. Energy loss and straggling should be minimized.

Besides the obvious easy sample handling and positioning in air, the use of an external beam provides several notable advantages:

1. Objects of large size and complex structure and shape can be analyzed *in situ* without the need of sampling, a fact particularly valuable for art objects.
2. It is possible to study materials containing volatile compounds that could otherwise not stand vacuum.
3. The risk of damage due to heating is considerably reduced because of efficient cooling by the air or the helium flow.
4. Charging of insulating materials is totally avoided without the need of the thin conductive coating required when operating under vacuum. Indeed, charging effects can produce potentials up to several tens of kilo-electron-volts and accelerate accordingly secondary electrons with a subsequent extension of the bremsstrahlung background to higher energy. The detection limit would then be markedly increased. Moreover, deposition of a conductive coating on a precious museum object would of course be prohibited.

The main difficulty when operating in the external beam mode is the precise determination of the integrated dose of particles that is needed for accurate analysis. Several means have been employed for beam monitoring: a beam chopper inside or outside the vacuum, the Ar X K_α line produced along the beam path in air, the X-ray or RBS signal of a major component of the target used as an internal standard, or a specific signal emitted by the exit foil, which can be gamma rays, X-rays, or backscattered particles. The latter seems to be the most reliable technique.

6.8.2. Microbeam

A common feature of analytical tools based on charged particles, whether they are electrons or ions, is the ability to focus the beam by means of elec-

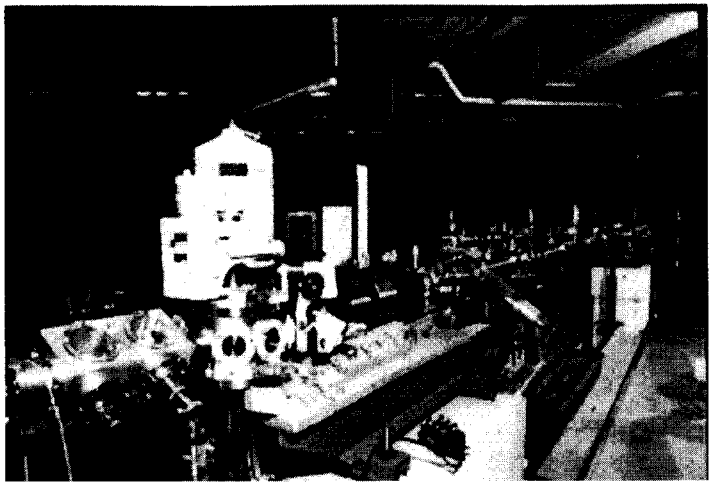

Figure 6.9. View of nuclear microprobe.

trostatic or magnetic lenses down to very small diameters, in the micrometer range for ions. The resulting instruments, which rely on mega-electron-volt ions, and a set of analytical techniques that include PIXE are called nuclear microprobes (Fig. 6.9), whereas those based on sputtering by kilo-electron-volt ions and mass spectrometry are named ion microprobes. The beam can be scanned over the sample in providing elemental micromapping with a high lateral resolution and even a three-dimensional distribution when using depth profiling techniques. The first nuclear microprobe was built at the end of the 1960s (Cookson et al. 1972), at the same time as the development of PIXE. Because of its high sensitivity, PIXE is well suited to the microprobe mode, but the relatively large probed depth (over 10 μm in most thick samples) excludes the need of beam focusing below 1 μm for the analysis of thick samples. Another limitation to the use of very narrow beams stems from the high density of energy deposited and the subsequent risk of damage. Nuclear microprobes are usually operated under vacuum, a fact that limits their usefulness for the analysis of objects of cultural heritage. However, it is generally admitted that applications of nuclear microprobes in art and archaeology do not require very high lateral resolution (Swann 1997) and that focused external beams of size around 50 μm are well adapted to this field. This type of set-up has been developed on the ion beam analysis facility of the Research Laboratory of the Museums of France in Paris (Calligaro et al. 1998a), which is named AGLAE, an acronym for Accélérateur Grand Louvre d'Analyse Elémentaire. The focusing system consists of three magnetic quadrupoles; previously this system was equipped with a microprobe built

by the Oxford proton microprobe unit (Watt and Grime 1987). It is worth describing below a few details of the set-up (Calligaro et al. 1996).

6.8.3. AGLAE External Beam Line

The beam conditions in the PIXE mode are currently a proton energy of 3 MeV, intensity of 1 nA (which can be reduced down to 50 pA for the study of paperlike materials), and diameter from about 0.1 to 1 mm for routine work. Two Si(Li) detectors are used to cover the entire X-ray energy range. They are set at 45° with respect to the beam direction, the one dedicated to major light elements (low-energy X-rays) in an horizontal plane and the second for trace elements (high-energy X-rays) in a vertical plane. Their characteristics are the following:

Low-Energy Detector. Active surface 10 mm^2, window made of 0.25-μm-thick boron nitride, filter of 0.5-μm C foil to stop the light; fitted with a 50-mm-long magnet to deflect backscattered protons; helium flow to fill the 70-mm long path between the beam spot and the detector.

High-Energy Detector. Active surface 50 mm^2; 5-μm-thick Be window; Al filter of thickness depending on the experiment, designed to stop backscattered protons and matrix X-rays; the distance to the spot can be as low as 15 mm. The detector is shielded against X-rays emitted by the exit window by means of a 1-mm-thick lead cover.

The beam line is terminated by a conical nozzle of about 120 mm length containing the exit window (Fig. 6.10). The nozzle can be accurately positioned with respect to the lens axis by means of a x–y micrometric stage, so that the beam hits the center of the exit window. The characteristics of the exit window depend on the type of analysis performed. Metallic foils have been preferred to previously used Kapton windows because of their much greater stability to radiations. For millimeter-sized beams, the exit window has an area of about 4 mm^2 and is made of a 10-μm Al foil. For micro-PIXE operation, we have successively obtained a beam spot of about 20 to 30 μm with a 0.75-μm-thick Al foil and of roughly 10 μm with a 0.1-μm-thick Si_3N_4 foil.

The beam monitoring usually relies on the detection of particles backscattered by the exit foil, which is tilted at 45° with respect to the beam and directly faces the surface barrier Si detector. Such a geometry permits an accurate monitoring, as the detector collects the entire signal even when the beam spot on the window is not well centered. However, when producing an external microbeam, the small thickness of the Al exit window and the subsequent extremely low count rate of backscattered particles exclude this

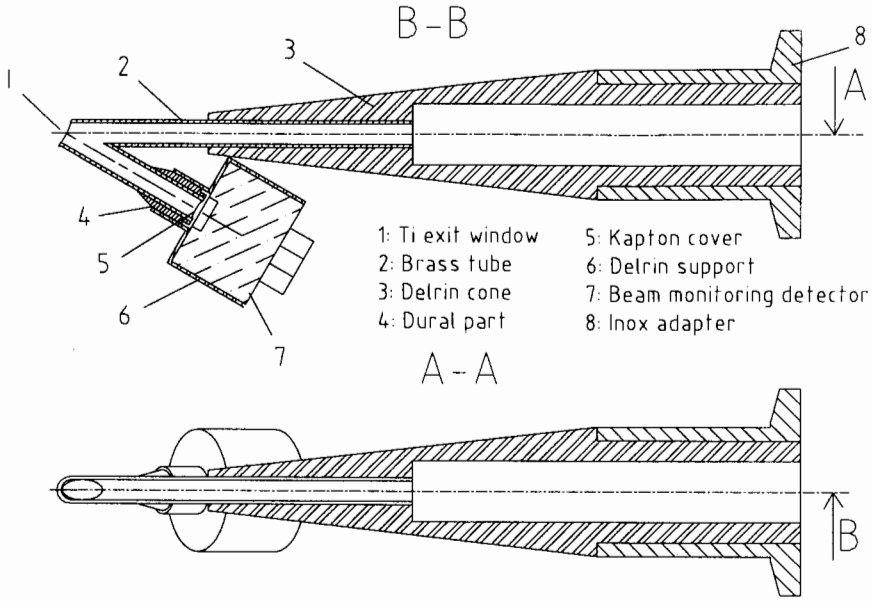

Figure 6.10. Cross section of exit nozzle of AGLAE external beam line.

monitoring method. The Al X-rays emitted by the window are more favorable, but the small dimensions of the nozzle do not fit a classical liquid-nitrogen-cooled Si(Li) detector and require a more compact detector cooled by Peltier effect.

The sample is placed as close as possible to the exit window in order to reduce the spot broadening due to the angular straggling induced by the window crossing. The minimum distance that allows X-ray detection with external Si(Li) detectors is about 3 mm. The sample position is remotely controlled with an accuracy of 0.1 mm by a set of laser beams and a video camera. The beam profiling has been performed by using a reference sample made of a cross section of a 2-μm Zr foil imbedded in aluminum and submitted to a linear scan with steps depending on the beam size. The Si(Li) detector dedicated to high-energy X-rays is used to record the K_α and K_β Zr lines.

6.9. EXAMPLES OF APPLICATIONS

Applications of PIXE in the field of art and archaeology started almost since the early development of the technique with the analysis of a pottery shard

(Gordon and Kraner 1972). They were quickly extended to all types of objects of the cultural heritage. However, because of the features described in Section 6.7, PIXE is more appropriate to some materials than to others. It is particularly suitable for the *in situ* analysis of thin layers of high-Z compounds on top of low-Z substrates. This ideal situation is encountered, for example, in drawings and illuminated manuscripts (Cahill et al. 1981; Kusko and Schwab 1987). In contrast, it is much more difficult to analyze easel paintings *in situ* without sampling, due to both the usual presence of a thick varnish coating and the complex structure of the paint layer. Recent efforts have been made to overcome this difficulty by using multiple-energy PIXE, which permits in some cases to identify the pigments and layer arrangement (Brissaud et al. 1996; Neelmeijer et al. 1996). Other materials are difficult to analyze *in situ*: metallic alloys because of the much higher detection limit than in light matrices and glasses because of the formation of an altered surface layer. It is out of the scope of the present chapter to provide a complete description of the numerous works published in the literature. Rather we will concentrate on the most recent ones dating from 1990 with particular emphasis on those performed in our laboratory. Instead of drawing a comprehensive list of applications classified according to the types of materials, as done elsewhere, we will stress the underlying issue of archaeology, art history, and conservation.

6.9.1. Materials Identification

Materials identification is the basic objective of the scientific characterization of museum objects and provides important clues for the knowledge of the fabrication procedure and the authentication of the work of art. This task is quite easily performed by PIXE in the external beam mode. This approach is illustrated by several investigations (Table 6.1) performed on manuscripts, miniatures, and drawings and intended to identify the nature of inks, metal points, and pigments. Important information was inferred on the use of pigments in medieval manuscripts: for instance, the very precious ultramarine blue, derived from lapis lazuli, has been surprisingly found on twentieth-century every-day mass books (McArthur et al. 1990). On Renaissance drawings by Pisanello, the use of different metal points was clearly evidenced (Duval 1997): lead or silver–mercury alloy on unprepared paper or parchment and pure silver on a preparation made of bone white and calcium carbonate. An interesting application of ink/pigment analysis on manuscripts concerns the enhanced visibility of faded characters through elemental mapping (Lovestam and Swietlicki 1990). Among numerous other works, we can also quote the identification of components of prestigious statues (Calligaro et al. 1998b) or jewels (Querré et al. 1996) kept in the Louvre in

Table 6.1. Materials Identification by PIXE Analysis of Major Elements

Artistic or Archaeological Objects	Component of Interest	Reference
Antique papyrus	Ink	Lovestam and Swietliki 1990
Medieval miniatures	Pigments	McArthur et al. 1990
		Bussotti et al. 1997
Medieval Copt manuscripts	Inks and pigments	McArthur 1995
Medieval and Renaissance manuscripts	Inks	Del Carmine et al. 1993
		Cambria et al. 1993
Historical manuscripts	Inks	Giuntini et al. 1995
		Del Carmine et al. 1996
Chinese ancient paper money	Seal ink	Wu et al. 1993
Renaissance book engravings	Pigments	Neelmeijer et al. 1995
Renaissance drawings	Metal points	Duval 1997
Egyptian pectorals	Gems	Bouquillon et al. 1992
Antique jewels	Gems	Querré et al. 1996
Antique statuette	Gems	Calligaro et al. 1998b

Paris. The first study, devoted to a Parthian statue representing the goddess of love Ishtar, allowed the authors to identify the inlays forming the eyes and navel as rubies and not colored glasses as previously assumed by the museum curators.

6.9.2. Materials Provenance

This issue is probably the most frequently addressed in archaeological works because it is the key toward the knowledge of ancient trade routes and links between populations. For many years it was almost the monopoly of instrumental neutron activation analysis (INAA) due to the high sensitivity of this technique for trace elements that constitute the fingerprint of the material source (see Chapter 5). Now PIXE and to a lesser extent XRF (X-ray fluorescence) have replaced INAA in the great majority of studies. The current methodology combines trace element analysis of artifacts and samples of well-defined geological sources and multivariate statistical methods that first identify the discriminant elements and permit to ascribe to each artifact a source with a calculated probability. This approach has been applied to numerous materials (see Table 6.2), including stones (obsidians, flints), gems (rubies, emeralds), and ceramics. An example is provided by the determination of the provenance of the ruby inlays of the above-mentioned statuette. PIXE spectra for both major and trace elements are reported in Figure 6.11. A large collection of rubies of well-known provenance has been submitted to

Table 6.2. Materials Provenancing by PIXE Analysis of Trace Elements

Artistic or Archaeological Objects	Material of Interest	Reference
Tool or arrowhead	Obsidian	Poupeau et al. 1996
Inlays of antique statuette	Ruby	Calligaro et al. 1998b
Medieval jewels	Garnet	Farges 1998
Potsherds from South Africa	Clay	Peisach et al. 1990
		Jacobson et al. 1994
		Bollong et al. 1997
Islamic and Chinese potteries	Porcelain	Fleming and Swann 1992
Italian medieval potteries	Clay	Zucchiatti et al. 1993
		Zucchiatti et al. 1998
Byzantine ceramics	Paste and glaze	Waksman et al. 1994

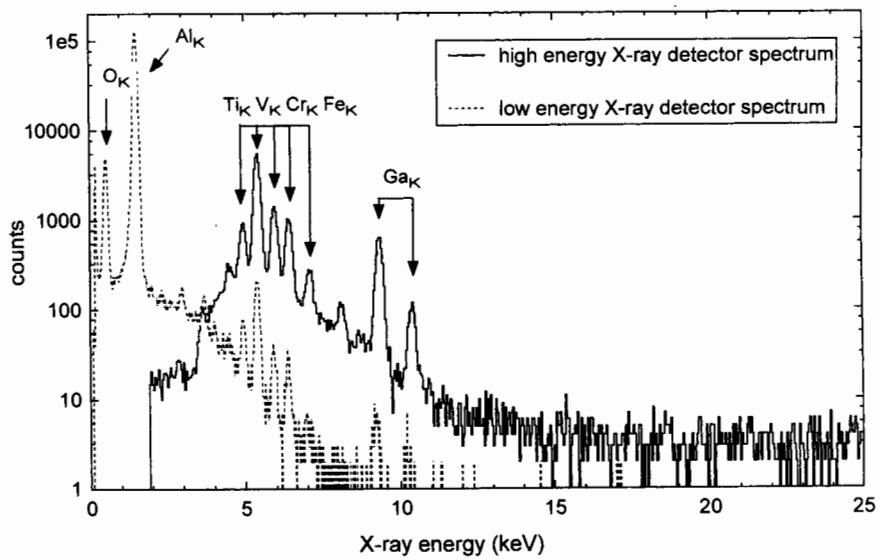

Figure 6.11. PIXE spectrum of rubies of Parthian statuette.

PIXE analysis under the same experimental conditions. Multivariate statistical processing of all data of elemental analysis was performed and led to the conclusion that the most likely provenance of the statuette rubies is Burma. The binary diagram in Figure 6.12 illustrates this statement.

In the case of ceramics, *in situ* analyses are seldom done because of potential bias due to their heterogeneous character. Therefore, most studies imply sampling a small amount of material that is ground and transformed

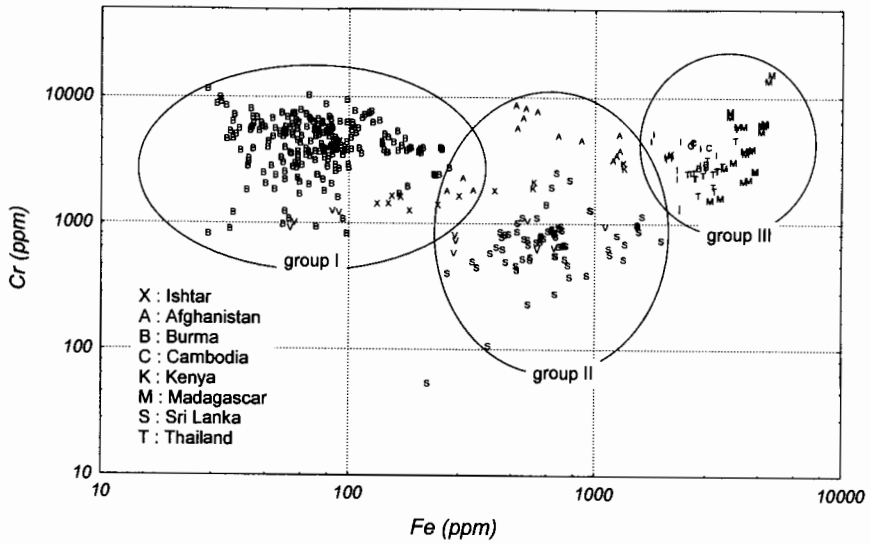

Figure 6.12. Binary diagram of Fe versus Cr contents in rubies of various provenances. Note that rubies of statuette of Fig. 6.11 fall inside first of three distinct groups.

into a flat pellet for measurement. Sometimes, the elemental composition is not sufficient to discriminate among potential sources, and thus an additional parameter can be helpful: for instance, for provenancing obsidian artifacts, the solidification age of obsidian inferred from fission track dating was decisive (Poupeau et al. 1996).

6.9.3. Information on the Fabrication Technology (Table 6.3)

Useful clues can indeed be extracted from the simple identification of materials used to make the work, but generally elemental distribution, either lateral or in-depth, is required. PIXE with good lateral resolution using a focused beam is thus preferable. A good illustration of the wealth of information that can be provided by PIXE analysis is the work of Demortier and co-workers on the soldering technology of gold jewelry of various origins (Demortier 1992, 1996).

6.10. CONCLUSION

PIXE has now reached its mature state and appears to be a very reliable analytical technique suited to almost all areas of research and technology. It

Table 6.3. Works Dealing with Fabrication Technology

Artistic or Archaeological Objects	Component of Interest	Reference
Panamanian gold artifacts	Au–Cu gilding	Fleming et al. 1990
Roman gold jewelry	Soldering joints	Weber et al. 1990
Antique and medieval gold artifacts	Soldering joints	Demortier 1992, 1996
Gold artifacts	Au–Cu alloy	Demortier and Rubalcaba-Sil 1996; Rubalcaba-Sil and Demortier 1996, 1997

combines several features, which explains its great popularity in art and archaeology: high sensitivity, nondestructive character, and rapidity and flexibility of implementation, particularly in the external beam mode. In fact, it is probably the most useful ion beam analysis technique in this field and served as the strongest argument for the construction of the AGLAE facility, which up to now is the only one in the world entirely devoted to the study of objects of cultural heritage. However, this technique has limitations and should not be considered a panacea. For the study of museum objects, its use should be restricted to investigations needing both high sensitivity and good lateral resolution. Otherwise, X-ray fluorescence could be substituted, as an alternative technique.

Acknowledgments

We thank J. P. Mohen for his constant support and interest in our work. We are also grateful to several of our colleagues: B. Moignard for his contribution to the improvement of the experimental set-up, A. Bouquillon and G. Querré for their pertinent comments and suggestions, and D. Bagault and D. Vigears for the photographs of the AGLAE facility.

REFERENCES

Anttila, A., J. Raisanen, and R. Lappalainen (1985), *Nucl. Instrum. Methods B* **12**, 245.

Bird., J. R., P. Duerden, and D. J. Wilson (1983), *Nucl. Sci. Applications B* **1**, 357.

Bollong, C. A., L. Jacobson, M. Peisach, C. A. Pineda, and C. G. Sampson (1997), *J. Archaeol. Sci.* **24**, 319.

Bouquillon, A., G. Querré, and J. P. Poirot (1992), *Proceedings of the Third International Conference on Non-Destructive Testing Microanalytical methods and*

environmental evaluation for study and conservation of Works of Art, M. Marabelli and P. Santopadre, eds. ICR-AIPhD-Beta Gamma, Rome, Italy.

Brandt, W., and G. Lapicki (1981), *Phys. Rev. A* **23**, 1717.

Breese, M. B. H., G. W. Grime, and F. Watt (1992), *Ann. Rev. Nucl. Part. Sci.* **42**, 1.

Brissaud, I., G. Lagarde, and P. Midy (1996), *Nucl. Instrum. Methods B* **117**, 179.

Bussotti, L., M. P. Carboncini, E. Castellucci, L. Giuntini, and P. A. Mando (1997), *Stud. Cons.* **42**, 83.

Cahill, T. A. (1980), *Ann. Rev. Nucl. Part. Sci.* **30**, 211.

Cahill, T. A., B. Kusko, and R. N. Schwab (1981), *Nucl. Instrum. Methods* **181**, 205.

Cahill, T. A., B. H. Kusko, R. A. Eldred, and R. N. Schwab (1984), *Archaeometry* 26, **3**.

Calligaro, T., J. D. MacArthur, and J. Salomon (1996), *Nucl. Instrum. Methods B* **109/110**, 125.

Calligaro, T., J. C. Dran, H. Hamon, B. Moignard, and J. Salomon (1998a), *Nucl. Instrum. Methods B* **136–138**, 339.

Calligaro, T., A. Mosmann, J.-P. Poirot, and G. Querré (1998b), *Nucl. Instrum. Methods B* **136–138**, 846.

Cambria, R., P. Del Carmine, M. Grange, F. Lucarelli, and P. A. Mando (1993), *Nucl. Instrum. Methods B* **75**, 488.

Campbell, J. L., A. Perujo, and B. M. Millman (1987), *X-ray Spectrom.* **16**, 195.

Campbell, J. L., D. Higushi, J. A. Maxwell, and W. J. Teesdale (1993), *Nucl. Instrum. Methods B* **77**, 95.

Campbell, J. L., G. K. Czamanske, L. MacDonald, and W. J. Teesdale (1997), *Nucl. Instrum. Methods B* **130**, 608.

Chadwick, J. (1912), *Philos. Mag.* **24**, 594.

Cheng, H., D. Yanfang, H. Wenquan, and Y. Fujia (1998), *Nucl. Instrum. Methods B* **136–138**, 897.

Cholewa, M., G. Brench, B. J. Kirby, and G. J. F. Legge (1991), *Nucl. Instrum. Methods B* **54**, 101.

Chu, W., J. Liu, Z. Zhang, and K. B. Ma (1994), in *Materials Science and Technology, Characterization of Materials*, Vol. 2B., E. Lifshin, Ed., VCH, Weinheim, p. 423.

Cohen, D. D., and E. Clayton (1989), in *Ion Beam for Materials Analysis*, J. R. Bird and J. S. William, Eds., Academic, Marrickville, NSW Australia, p. 209.

Cookson, J. A. (1988), *Nucl. Instrum. Methods B* **30**, 324.

Cookson, J. A., A. T. G. Ferguson, and F. D. Pilling (1972), *J. Radioanal. Chem.* **12**, 39.

Deconninck, G., and F. Bodart (1978), *Nucl. Instrum. Methods* **149**, 609.

Del Carmine, P., F. Lucarelli, P. A. Mando, and A. Pecchioli (1993), *Nucl. Instrum. Methods B* **75**, 480.

Del Carmine, P., L. Giuntini, W. Hooper, F. Lucarelli, and P. A. Mando (1996), *Nucl. Instrum. Methods B* **113**, 354.

Demortier, G. (1991), *Nucl. Instrum. Methods B* **54**, 334.

Demortier, G. (1992), *Nucl. Instrum. Methods B* **64**, 481.

Demortier, G. (1996), *Nucl. Instrum. Methods B* **113**, 347.

Demortier, G., and J. L. Rubalcaba-Sil (1996), *Nucl. Instrum. Methods B* **118**, 352.

Duval, A. (1997), *Proceedings of the Fifth International Conference on Non-Destructive Testing Microanalytical methods and environmental evaluation for study and conservation of Works of Art*, M. Marabelli and C. Parisi, eds., AIPhD-ICR, Rome, Italy.

Farges, F. (1998), *Am. Mineral.* **83**, 323.

Fleming, S. J., and C. P. Swann (1992), *Nucl. Instrum. Methods B* **64**, 528.

Fleming, S. J., C. P. Swann, P. E. McGovern, and L. Horne (1990), *Nucl. Instrum. Methods B* **49**, 293.

Garcia, J. D., R. J. Fortner, and T. M. Kavanagh (1973), *Rev. Mod. Phys.* **45**, 111.

Giuntini, L., F. Lucarelli, P. A. Mando, W. Hooper, and P. H. Barker (1995), *Nucl. Instrum. Methods B* **95**, 389.

Gordon, G. M., and H. W. Kraner (1972), *J. Radioanal. Chem.* **12**, 181.

Jacobson, L., C. A. Pineda, D. Morris, and M. Peisach (1994), *Nucl. Instrum. Methods B* **85**, 901.

Janssens, K., A. Aerts, L. Vincze, F. Adams, C. Yang, R. Utui, K. Malmqvist, K. W. Jones, M. Radtke, S. Garbe, F. Lechtenberg, A. Knochel, and H. Wouters (1996), *Nucl. Instrum. Methods B* **109/110**, 690.

Johansson, G. (1982), *X-ray Spectrom.* **11**, 194.

Johansson, S. A. E., and J. L. Campbell (1988), *PIXE: A Novel Technique for Elemental Analysis*, Wiley, New York.

Johansson, S. A. E., and T. B. Johansson (1976), *Nucl. Instrum. Methods* **137**, 473.

Johansson, S. A. E., J. L. Campbell, and K. G. Malqvist (1995), *Particle Induced X-ray Emission Spectrocopy (PIXE)*, John Wiley & Sons, New York.

Johansson, T. B., K. R. Akselsson, and S. A. E. Johansson (1970), *Nucl. Instrum. Methods* **84**, 141.

Katsanos, A., A. Xenoulis, A. Hadjhantoniou, and R. W. Fink (1976), *Nucl. Instrum. Methods* **137**, 119.

Kusko, B. H., and R. N. Schwab (1987), *Nucl. Instrum. Methods B* **22**, 401.

Lovestam, N. E. G., and E. Swietlicki (1990), *Nucl. Instrum. Methods B* **45**, 307.

Maeda, K., K. Hasegawa, H. Hamanaka, and K. Ogiwara (1998), *Nucl. Instrum. Methods B* **134**, 418.

Mando, P. A. (1994), *Nucl. Instrum. Methods B* **85**, 815.

Maxwell, J. A., J. L. Campbell, and W. J. Teesdale (1988), *Nucl. Instrum. Methods B* **43**, 218.

McArthur, J. D. (1995), *Techne* **2**, 68.

McArthur., J. D., P. Del Carmine, F. Lucarelli, and P. A. Mando (1990), *Nucl. Instrum. Methods B* **45**, 315.

McColm, D. W., and T. A. Cahill (1991), *Nucl. Instrum. Methods B* **54**, 91.

Mitchell, I. V., and K. M. Barfoot (1981), *Nucl. Sci. Applications* **1**, 99.

Neelmeijer, C., W. Wagner, H. P. Schramm, and U. Thiel (1995), *Nucl. Instrum. Methods B* **99**, 390.

Neelmeijer, C., W. Wagner, and H. P. Schramm (1996), *Nucl. Instrum. Methods B* **118**, 338.

Peisach, M. (1987), *J. Radioanal. Nucl. Chem.* **110**, 461.

Peisach, M., C. A. Pineda, and L. Jacobson (1990), *Nucl. Instrum. Methods B* **49**, 309.

Potts, P. J. (1987), in *A Handbook of Silicate Rock Analysis*, Blackie, Glasgow, p. 286.

Poupeau, G., L. Bellot-Gurlet, O. Dorighel, T. Calligaro, J.-C. Dran, and J. Salomon (1996), *C. R. Acad. Sci. Paris* **323**, 443.

Querré, G., A. Bouquillon, T. Calligaro, M. Dubus, and J. Salomon (1996), *Nucl. Instrum. Methods B* **109/110**, 686.

Raisanen, J. (1984), *Nucl. Instrum. Methods B* **3**, 220.

Rauhala, E., and J. Raianen (1985), *Nucl. Instrum. Methods B* **12**, 321.

Rubalcaba-Sil, J. L., and G. Demortier (1996), *Nucl. Instrum. Methods B* **113**, 275.

Rubalcaba-Sil, J. L., and G. Demortier (1997), *Nucl. Instrum. Methods B* **130**, 297.

Scuti, S., and G. Suber (1991), *Rivista Nuovo Cimento* **14**, 1.

Seaman, G. G., and K. C. Shane (1975), *Nucl. Instrum. Methods* **126**, 473.

Swann, C. P. (1997), *Nucl. Instrum. Methods B* **130**, 289.

Swann, C. P., and S. J. Fleming (1990), *Nucl. Instrum. Methods B* **49**, 65.

Waksman, S. Y., A. Pape, and Ch. Heitz (1994), *Nucl. Instrum. Methods B* **85**, 824.

Watt, F., and G. W. Grime (1987), *Principles and Applications of High-Energy Ion Microbeams*, Adam Hilger, Bristol.

Weber, J., Th. Beier, U. Diehl, D. Lambrecht, H. Mommsen, and F. J. Pantenburg (1990), *Nucl. Instrum. Methods B* **50**, 221.

Williams, E. T. (1984), *Nucl. Instrum. Methods B* **3**, 211.

Wu, X., X. Zeng, and F. Yang (1993), *Nucl. Instrum. Methods B* **75**, 458.

Zeng, X., X. Wu, Q. Shao, J. Tang, and F. Yang (1990), *Nucl. Instrum. Methods B* **47**, 143.

Zeng, X., X. Wu, H. Yao, F. Yang, and T. A. Cahill (1993), *Nucl. Instrum. Methods B* **75**, 99.

Zucchiatti, A., H. J. Annegarn, M. A. Kneen, and C. Varaldo (1993), *Nucl. Instrum. Methods B* **75**, 463.

Zucchiatti, A., F. Cardoni, P. Prati, F. Lucarelli, P. A. Mando, and G. P. Martino (1998), *Nucl. Instrum. Methods B* **136–138**, 893.